Cassini observations of ion and electron beams at Saturn and their relationship to infrared auroral arcs

S. V. Badman,[1] N. Achilleos,[2,3] C. S. Arridge,[3,4] K. H. Baines,[5] R. H. Brown,[6] E. J. Bunce,[7] A. J. Coates,[3,4] S. W. H. Cowley,[7] M. K. Dougherty,[8] M. Fujimoto,[1] G. Hospodarsky,[9] S. Kasahara,[1] T. Kimura,[1] H. Melin,[7] D. G. Mitchell,[10] T. Stallard,[7] and C. Tao[1]

Received 6 October 2011; revised 17 November 2011; accepted 7 December 2011; published 21 January 2012.

[1] We present Cassini Visual and Infrared Mapping Spectrometer observations of infrared auroral emissions from the noon sector of Saturn's ionosphere revealing multiple intense auroral arcs separated by dark regions poleward of the main oval. The arcs are interpreted as the ionospheric signatures of bursts of reconnection occurring at the dayside magnetopause. The auroral arcs were associated with upward field-aligned currents, the magnetic signatures of which were detected by Cassini at high planetary latitudes. Magnetic field and particle observations in the adjacent downward current regions showed upward bursts of 100–360 keV light ions in addition to energetic (hundreds of keV) electrons, which may have been scattered from upward accelerated beams carrying the downward currents. Broadband, upward propagating whistler waves were detected simultaneously with the ion beams. The acceleration of the light ions from low altitudes is attributed to wave-particle interactions in the downward current regions. Energetic (600 keV) oxygen ions were also detected, suggesting the presence of ambient oxygen at altitudes within the acceleration region. These simultaneous in situ and remote observations reveal the highly energetic magnetospheric dynamics driving some of Saturn's unusual auroral features. This is the first in situ identification of transient reconnection events at regions magnetically conjugate to Saturn's magnetopause.

Citation: Badman, S. V., et al. (2012), Cassini observations of ion and electron beams at Saturn and their relationship to infrared auroral arcs, *J. Geophys. Res.*, *117*, A01211, doi:10.1029/2011JA017222.

1. Introduction

[2] Early observations of Saturn's aurorae at ultraviolet (UV) wavelengths suggested they formed a narrow (1–2°) "main oval" ring of emission circling the poles at ∼20° colatitude [*Broadfoot et al.*, 1981]. Interpretation of auroral images combined with modeling and in situ measurements have demonstrated that Saturn's main oval emissions are generated by a field-aligned current system associated with the boundary between open and closed magnetic field lines [*Cowley et al.*, 2004; *Badman et al.*, 2006; *Belenkaya et al.*, 2007; *Bunce et al.*, 2008a]. In this scenario, the area poleward of the main auroral oval maps to open field lines, and its size is determined by the balance between opening of flux at the dayside magnetopause and closure in the magnetotail, similar to the terrestrial case.

[3] While most of the past studies of Saturn's aurorae have been made in the UV, especially by the Hubble Space Telescope, high spatial resolution images of Saturn's infrared (IR) aurora have been available from the Visual and Infrared Mapping Spectrometer (VIMS) [*Brown et al.*, 2004] on board Cassini. For simplicity throughout this study, the term "IR aurora" is used to denote H_3^+ auroral emission, as the wavelength ranges used were dominated by H_3^+ emission lines. To generate IR H_3^+ emissions, incident auroral electrons ionize atmospheric H_2 to form H_2^+, which then reacts with H_2 to produce the H_3^+ ionized molecule. Ro-vibrational transitions of the H_3^+ molecule, which has a lifetime of ∼500 s [*Melin et al.*, 2011], produce the IR auroral emissions [*Drossart et al.*, 1989]. H_3^+ emissions are strongly dependent on the background temperature and incident electron energy and flux [*Tao et al.*, 2011]. Recent analyses of auroral images taken by Cassini have shown Saturn's main IR auroral emissions to be colocated with those in the UV and thus

[1]JAXA Institute of Space and Astronautical Science, Sagamihara, Japan.
[2]Department of Physics and Astronomy, University College London, London, UK.
[3]Centre for Planetary Sciences at UCL/Birkbeck, London, UK.
[4]Mullard Space Science Laboratory, University College London, Dorking, UK.
[5]SSEC, University of Wisconsin–Madison, Madison, Wisconsin, USA.
[6]LPL, University of Arizona, Tucson, Arizona, USA.
[7]Department of Physics and Astronomy, University of Leicester, Leicester, UK.
[8]Blackett Laboratory, Imperial College London, London, UK.
[9]Department of Physics and Astronomy, University of Iowa, Iowa City, Iowa, USA.
[10]APL, Johns Hopkins University, Laurel, Maryland, USA.

0148-0227/12/2011JA017222

driven by the same field-aligned current system [*Badman et al.*, 2011a; *Melin et al.*, 2011].

[4] Detailed studies of Saturn's aurora have revealed a variety of morphologies more complicated than a discrete main oval, which have been related to both the solar wind conditions and the rotation of the planet [*Clarke et al.*, 2005, 2009; *Crary et al.*, 2005; *Grodent et al.*, 2005, 2011; *Nichols et al.*, 2010]. Some of the most intriguing time-dependent features are the localized "blobs" and enhanced arcs observed in the noon region, which have been termed Saturn's cusp aurora by analogy with observations of the Earth's aurora. These features are directly related to the interaction of Saturn's magnetosphere with the solar wind [*Gérard et al.*, 2004, 2005; *Bunce et al.*, 2005a]. Transient infrared emissions are commonly observed poleward of the main oval region and are usually diffuse, but can cover a range of sizes from small patches to large-scale "infilling" of the polar region [*Stallard et al.*, 2004, 2008; *Badman et al.*, 2011a, 2011b]. In this study we report, for the first time, an IR auroral configuration comprising multiple, distinct arcs poleward of the main oval in the noon sector.

[5] In situ observations of transient reconnection events have not been commonly detected at Saturn's magnetopause, unlike spacecraft encounters with the magnetopauses at Earth [*Rijnbeek et al.*, 1984], Mercury [*Slavin et al.*, 2008] and Jupiter [*Walker and Russell*, 1985]. However, evidence of reconnection in the form of a magnetic field component normal to Saturn's magnetopause [*Huddleston et al.*, 1997] and additional heated ion and electron populations [*McAndrews et al.*, 2008] have been presented. The location and rate of reconnection depend on the plasma beta parameter on both sides of the magnetopause, the interplanetary magnetic field (IMF) strength and orientation and the velocity of the solar wind [*Swisdak et al.*, 2003; *Jackman et al.*, 2004; *Bunce et al.*, 2006]. These latter parameters have also been shown to influence the large-scale behavior of Saturn's aurora [*Badman et al.*, 2005; *Cowley et al.*, 2005; *Grodent et al.*, 2005].

[6] *Bunce et al.* [2005a] modeled the effects of different IMF conditions on the ionospheric flows and current systems resulting from pulsed reconnection at both high latitudes and the subsolar magnetopause. As described in their model, at Saturn where the planetary field is oriented opposite to that of the Earth, reconnection at the subsolar magnetopause is expected to occur under conditions of northward IMF and will produce the following phenomena: (1) antisunward ionospheric flows and currents in the vicinity of the open-closed boundary (main oval); (2) the opening of dayside magnetic field lines; and (3) the expansion of the dayside auroral oval to lower latitudes. Conversely, high-latitude lobe reconnection would occur under prolonged southward IMF and result in reversed vortical flows and currents poleward of the open-closed boundary in the ionosphere. Subsolar reconnection is thus related to the intensification of the main auroral arc in the noon region, while high-latitude reconnection is related to localized auroral emission poleward of the main oval, whose distributions will be affected by the time development of the reconnection [*Bunce et al.*, 2005a; *Gérard et al.*, 2005].

[7] Observations of local processes related to Saturn's aurora have also been made in situ by the Cassini plasma instruments. *Saur et al.* [2006] identified beams of 20–800 keV electrons accelerated upward from Saturn's ionosphere in the predawn and noon sectors (the local time (LT) sector explored by Cassini during the studied orbits) and at radial distances of 11–20 R_S. Similar beams have also been described by *Mitchell et al.* [2009a], who simultaneously identified energetic upward ions (30–200 keV) and magnetic field perturbations. *Mitchell et al.* [2009a] interpreted these as the signatures of downward current layers, which were detected at dipole L shells of 10–50, i.e., incorporating the statistical auroral and polar cap regions. The events identified by *Mitchell et al.* [2009a] were observed at a range of local times and could be either steady for hours or pulsed with a repetition period of tens of minutes. While the discrete aurora are produced by electrons accelerated downward into the ionosphere (i.e., upward current regions), such downward directed current layers (energetic, upward traveling electrons) have also been identified in the auroral regions at Earth [*Carlson et al.*, 1998; *Marklund*, 2009] and Jupiter [*Mauk and Saur*, 2007]. Such current layers evidently play an integral role in energy transport in the auroral regions of these magnetized planets.

[8] In this study, in situ measurements of these distinctive downward current signatures are presented with, for the first time, a simultaneous image of the magnetically conjugate auroral region. This enables a direct comparison of the field-aligned currents evident in the magnetic field and plasma data with the resulting auroral features. In the following sections, the auroral morphology is described and then related to the relevant in situ plasma and magnetic field measurements.

2. Interval Overview: 2008 Day of Year 320 (15 November 2008)

[9] On day of year 320 of 2008 (15 November 2008) (hereafter 2008-320) Cassini moved inbound from the dayside magnetosphere at high northern latitudes. The trajectory for days of year (DOY) 318–324 in 2008 is shown in Figure 1 in the X-Y and X-Z planes in Kronocentric Solar Magnetospheric (KSM) coordinates, where X points from Saturn to the Sun, Y is positive toward dusk and the X-Z plane contains the planetary spin (and magnetic) axis. The ionospheric magnetic footprint of Cassini's trajectory is also shown in Figure 1 (right), with the sunward direction toward the right and dawn toward the bottom. The trajectory has been mapped from Cassini's magnetospheric position using the SOI model of Saturn's magnetic field [*Dougherty et al.*, 2005] and a model ring current field perturbation [*Bunce et al.*, 2007]. The ring current perturbation was modeled assuming a nominal magnetopause standoff distance of 21 R_S and the mapping was performed to 1100 km above the 1 bar reference spheroid. From 12:00 to 24:00 UT on day 320, Cassini was at a radial distance of $\sim$12 R_S, slightly duskward of noon, and moving toward the Northern Hemisphere at high latitude. This trajectory thus afforded an excellent view of the northern auroral region for Cassini imaging instruments.

2.1. Infrared Auroral Images

[10] A mosaic of six images of the northern IR aurora taken by VIMS on day 320 is shown in Figure 2a. VIMS acquires a full wavelength spectrum (0.85–5.1 μm) at each pixel position in its field of view (FOV) in turn, where

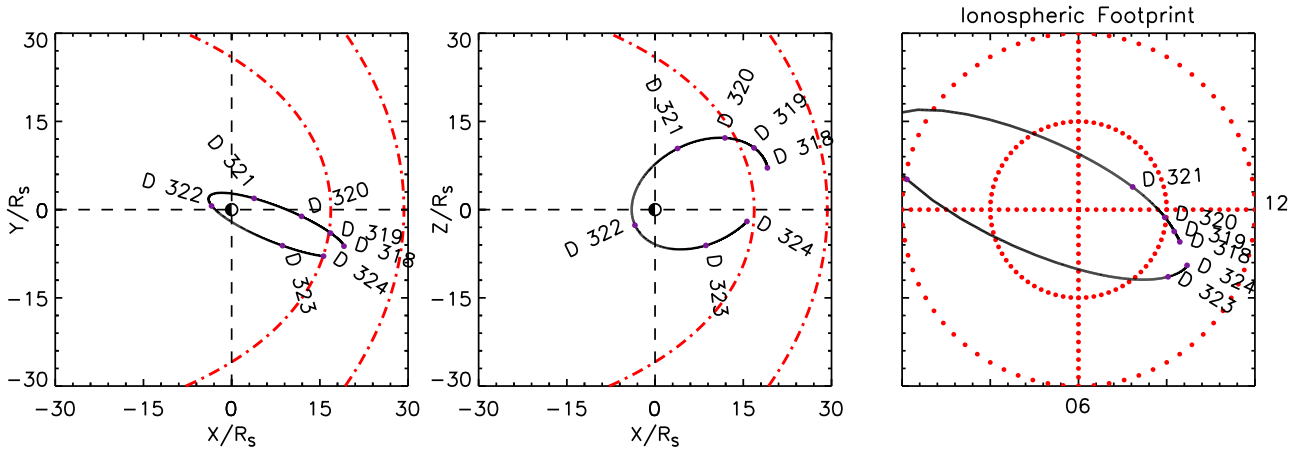

Figure 1. (left and middle) Cassini's trajectory and mapped northern ionospheric footprint during 2008 DOYs 318–324 (13–19 November 2008) in KSM coordinates, where X points from Saturn to the Sun, Y is positive toward dusk, and the X-Z plane contains the rotation (and magnetic) axis. The dot-dashed red lines indicate the extreme positions of the magnetopause for solar wind dynamic pressures of 0.01 nPa and 0.1 nPa, obtained from the *Arridge et al.* [2006] model. (right) The ionospheric footprint of Cassini's trajectory with the sunward direction toward the right and dawn toward the bottom. The red dots mark latitudes at intervals of 10° and the noon-midnight and dawn-dusk meridians.

1 pixel = 0.5 × 0.5 mrad and the FOV for these observations was 42 × 42 pixels. The total exposure time for each image was ∼30 min. The images in Figure 2 have been projected onto a 0.25° × 0.25° planetocentric polar grid using an estimated peak emission height of 1100 km above the 1 bar reference spheroid (T. S. Stallard et al., Peak emission altitude of Saturn's H_3^+ aurora, unpublished manuscript, 2011). The orientation is such that the observer is looking down onto the pole with the sunward direction (12:00 LT) at the bottom, dawn (06:00 LT) to the left and dusk (18:00 LT) to the right. The start time of each exposure (UT) is labeled on each image: 19:46 UT, 20:18 UT, 21:58 UT, 22:31 UT, 23:05 UT, and 23:38 UT.

[11] The data are color-coded according to specific intensity, and grey regions are those outside the VIMS FOV. Five nonconsecutive VIMS wavelength channels containing emission lines in the range 3.4–3.7 μm have been added to produce these images. The intensities have been corrected for line-of-sight effects using a simple cosine correction (i.e., multiplication by the cosine of the emission angle for each

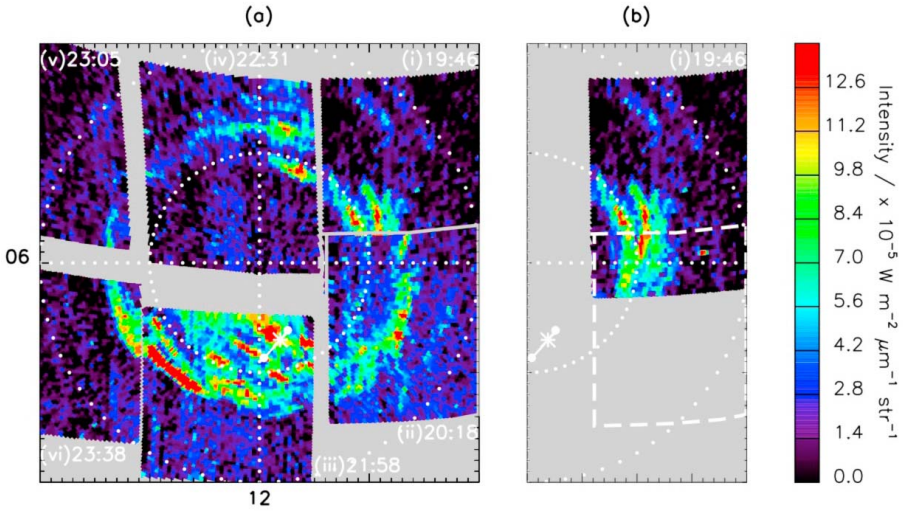

Figure 2. (a) A mosaic of six Cassini VIMS images of Saturn's infrared aurora taken on 2008-320. The start time of each image is marked at its edge: (i) 19:46 UT, (ii) 20:18 UT, (iii) 21:58 UT, (iv) 22:31 UT, (v) 23:05 UT and (vi) 23:38 UT. The white grid marks latitudes at intervals of 10° and the noon-midnight and dawn-dusk meridians. The white line delimited by dots shows Cassini's ionospheric footprint during 12:00–24:00 UT on 2008-320. The white asterisk marks Cassini's footprint at 22:00 UT on DOY 320. (b) Image i taken by Cassini VIMS showing the area overlapped by the following image ii whose outline is marked by the white dashed line. Cassini's ionospheric footprint is shown again here for clarity.

pixel) and are given in units of 10^{-5} W m^{-2} μm^{-1} sr^{-1}. The white line shows the ionospheric footprint of Cassini, mapped from the magnetosphere as described above to 1100 km above the 1 bar reference spheroid in order to match the auroral projection. White dots mark the ends of the trajectory at 12:00 UT and 24:00 UT on 2008-320. The white asterisk marks the footprint of Cassini at 22:00 UT on 2008-320, i.e., the time that image iii of this region was taken.

[12] Over the ~4 h imaging interval, intense and unusual auroral features were observed. The FOV of the first two images which had start times of 19:46 UT and 20:18 UT partially overlapped, as indicated by the grey outline of the later image in Figure 2a. Image for time i is therefore reproduced in Figure 2b, with the outline of the following image (image ii) indicated by the dashed white line for reference. Cassini's ionospheric footprint is also reproduced for clarity in Figure 2b. Considering this first image (image i), a wide auroral feature was observed on the dusk side extending between ~9°–13° colatitude and across most of the VIMS FOV: ~17:00–21:00 LT. The same region captured in image ii shows a narrower (~2°) auroral arc, located further from the pole to 13°–14° colatitude. Comparison of Figures 2a and 2b indicates that the intense feature around 18:00 LT evident in image i had either dimmed or rotated out of the FOV by the time of image ii. In image iii multiple, discrete arcs were observed in the noon region across 5°–13° colatitude. The arcs varied in width and longitudinal extent but were approximately 1° wide and separated by dark regions. The main oval, taken to be the lowest latitude arc, was very intense (several times greater than average [*Badman et al.*, 2011b]) in the prenoon region.

[13] The next two images which started at 22:31 UT and 23:05 UT show sections of the nightside aurora, where auroral arcs were also visible but at lower intensities than on the dayside. The two arcs present premidnight in image iv could plausibly be the extremity of the same feature observed in image i, after rotation round to the nightside at ~50% of the planetary rotation rate. The last image in the sequence (image vi) started at 23:38 UT and reveals an intense portion of the main oval postdawn and at slightly lower latitude than the adjacent image iii. The difference in start time between images iii and vi was 100 min.

[14] The trajectory plotted in Figure 2 shows that Cassini was sampling field lines mapping to the high-latitude noon sector during this interval. Image iii reveals a snapshot of the conjugate auroral morphology starting at 21:58 UT, while the other images which cover different LT ranges reveal the global dynamics during the interval.

[15] Overall this sequence reveals a dynamic aurora, with possible rotating features (e.g., the postdusk feature seen in image i), equatorward expansion of the oval on the dayside, and intense arcs poleward of the main oval, all occurring over an interval of less than 5 h. The discrete poleward arcs around noon are uncommon in the VIMS data set. Multiple auroral arcs have been identified in 6 out of 50 sequences of VIMS images studied so far, where two of these identifications were made in the noon sector. The morphology of these arcs is similar to bifurcations of the dayside auroral oval seen at the Earth, which are identified as the ionospheric signatures of newly opened flux tubes created by dayside reconnection [*Milan et al.*, 2000]. The apparent equatorward expansion of the dayside auroral oval seen in this sequence of VIMS images indicates an increase in open flux, thus supporting this interpretation. The temporal evolution of similar bifurcation features has recently been identified in UV images of Saturn's aurora by *Radioti et al.* [2011], who related them to transient dayside reconnection events based on their morphology compared with features seen at Earth. In sections 2.2–2.4 the in situ measurements acquired on 2008-320 are described in relationship to the VIMS auroral observations and the validity of our proposed transient reconnection interpretation is discussed.

2.2. Magnetic Field and Plasma Overview

[16] The electron and magnetic field measurements acquired by Cassini at 12:00–24:00 UT on 2008-320 are plotted in Figure 3. This corresponds to the duration of the trajectory drawn on the auroral images in Figure 2a. Figure 3 (top) shows an energy-time spectrogram of electron differential energy flux measured by the Cassini Plasma Spectrometer–Electron Spectrometer (CAPS-ELS) [*Young et al.*, 2004]. The electron energy range covered was 0.5 eV to 28 keV and the fluxes of field-perpendicular (pitch angles 80°–100°) electrons are plotted. Figure 3 (bottom) displays the components of the magnetic field in spherical radial (r), polar (θ) and azimuthal (ϕ) coordinates referenced to the spin (and magnetic) axis, from which the Cassini model of the internal planetary field [*Dougherty et al.*, 2005] has been subtracted. The arrows labeled i–vi at the top of Figure 3 (top) indicate the start times of the VIMS images shown in Figure 2a.

[17] At the start of the interval shown the warm (~100–1000 eV) electron population and small-scale fluctuations in the magnetic field components were suggestive of Cassini being on closed field lines. Cassini was at high latitudes at this time (~50°–55°) on field lines mapping to ~9°–8° colatitude. At around 17:30 UT the plasma and field data abruptly changed; there was a significant decrease in the electron flux at all energies except at <~10 eV (spacecraft photoelectrons), which may be indicative of the spacecraft crossing from closed to open field lines, and the B_ϕ component in particular showed sharp fluctuations. These fluctuations in B_ϕ occurred on ~1 h timescales, distinctly shorter than the well-known ~11 h "planetary period" oscillations. Perturbations of this nature in B_ϕ are indicative of field-aligned currents [*Talboys et al.*, 2011], the nature of which will now be investigated.

2.3. Field-Aligned Currents

[18] The equatorward directed height-integrated Pedersen current in the ionosphere I_P can be related via Ampère's law to the B_ϕ component of the magnetic field measured in the magnetosphere by

$$I_P = \pm \frac{\rho B_\phi}{\mu_0}, \quad (1)$$

where ρ is the cylindrical radial distance of Cassini from Saturn's spin axis and the negative sign applies for the Northern Hemisphere [e.g., *Bunce et al.*, 2008b; *Talboys et al.*, 2011]. This relationship assumes the current ring is azimuthally symmetric, which may not be the case for the features studied here but is taken as a reasonable first

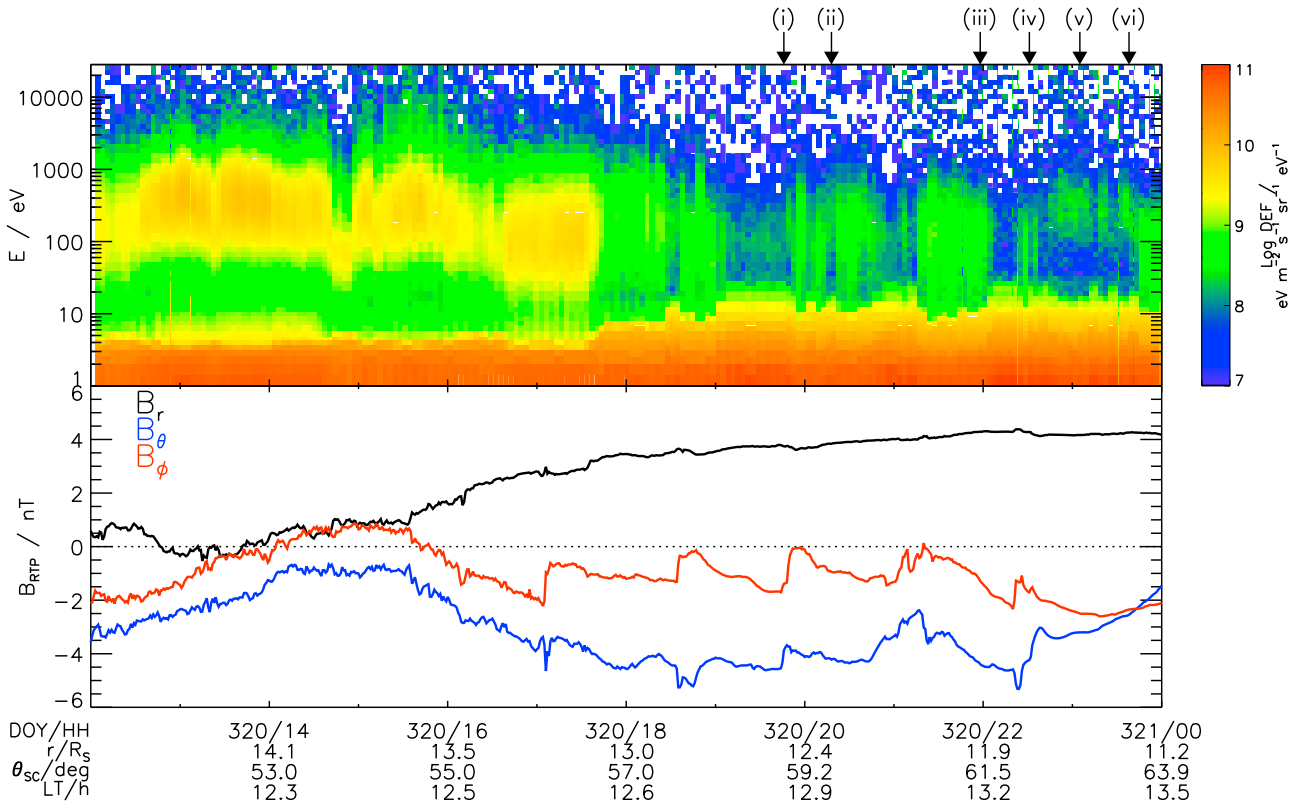

Figure 3. Overview of electron and magnetic field measurements made by Cassini during 12:00–24:00 UT on 2008-320. (top) The field-perpendicular electron differential energy flux spectrogram from ELS. (bottom) The residual (planetary field model subtracted) components of the magnetic field in spherical radial, polar and azimuthal coordinates. The labeled arrows at the top indicate the start times of the VIMS auroral images i–vi shown in Figure 2a.

estimate. B_ϕ and the calculated I_P are shown for the 12 h interval of interest (12:00–24:00 UT) in Figure 4 (first and third panels). The magnetically mapped ionospheric colatitude of Cassini is plotted in Figure 4 (second panel). The ~1 nT fluctuations in B_ϕ are apparent, as are the related increases and decreases in I_P. These fluctuations in I_P indicate currents flowing into or out of the ionosphere. Moving equatorward (right to left in Figure 4), a decrease in I_P requires an upward field-aligned current and an increase in I_P requires a downward field-aligned current. Regions of net decreases and increases in I_P have been marked by the vertical dashed lines in Figure 4 and labeled a–j, although smaller-scale fluctuations are also apparent within these regions.

[19] The net upward and downward directed currents ΔI in each of the regions a–j have been calculated and plotted in Figure 4 (fourth panel). Positive and negative values indicate upward and downward field-aligned currents, respectively. The upward and downward currents have similar magnitudes of 0.2–0.6 MA rad^{-1} but the downward current regions are narrower by a factor of 2–9. This implies that the current densities are higher in the downward current regions. The current density just above the ionosphere is calculated using

$$j_{\parallel I} = \frac{\Delta I}{R_i^2(\theta_i)\sin\theta_i \Delta\theta_i}, \qquad (2)$$

where R_i is the radius of the ionosphere at colatitude θ_i, calculated using an auroral surface 1100 km above the 1 bar oblate reference spheroid, and $\Delta\theta_i$ is the colatitudinal width of the region through which current ΔI flows in the ionosphere [e.g., *Bunce et al.*, 2008b]. The derived values are plotted for regions a–j in Figure 4 (fifth panel). The upward current densities are a few hundred nA m^{-2} and the downward current densities are larger, up to ~2000 nA m^{-2}. This analysis assumes that the features were stationary such that their width was measured by Cassini's motion across them. In fact, as will be discussed further below, the features may be significantly wider than the values obtained here and moving faster in the ionosphere than Cassini's footprint. This means that the current density values obtained here may be overestimated by a factor which depends on the real width of the moving features. Opposing this effect is the fact that the sharpest changes in B_ϕ occur over shorter timescales (or smaller spatial regions) than the broad current regions a–j defined above. This means that the current density would be higher than the derived values but in correspondingly smaller regions.

[20] This analysis of the magnetic field perturbations indicates that adjacent layers of intense upward and downward field-aligned currents were encountered by Cassini during this interval. The asymmetric nature of the signatures (i.e., steep increase, gradual decrease) suggests that this was

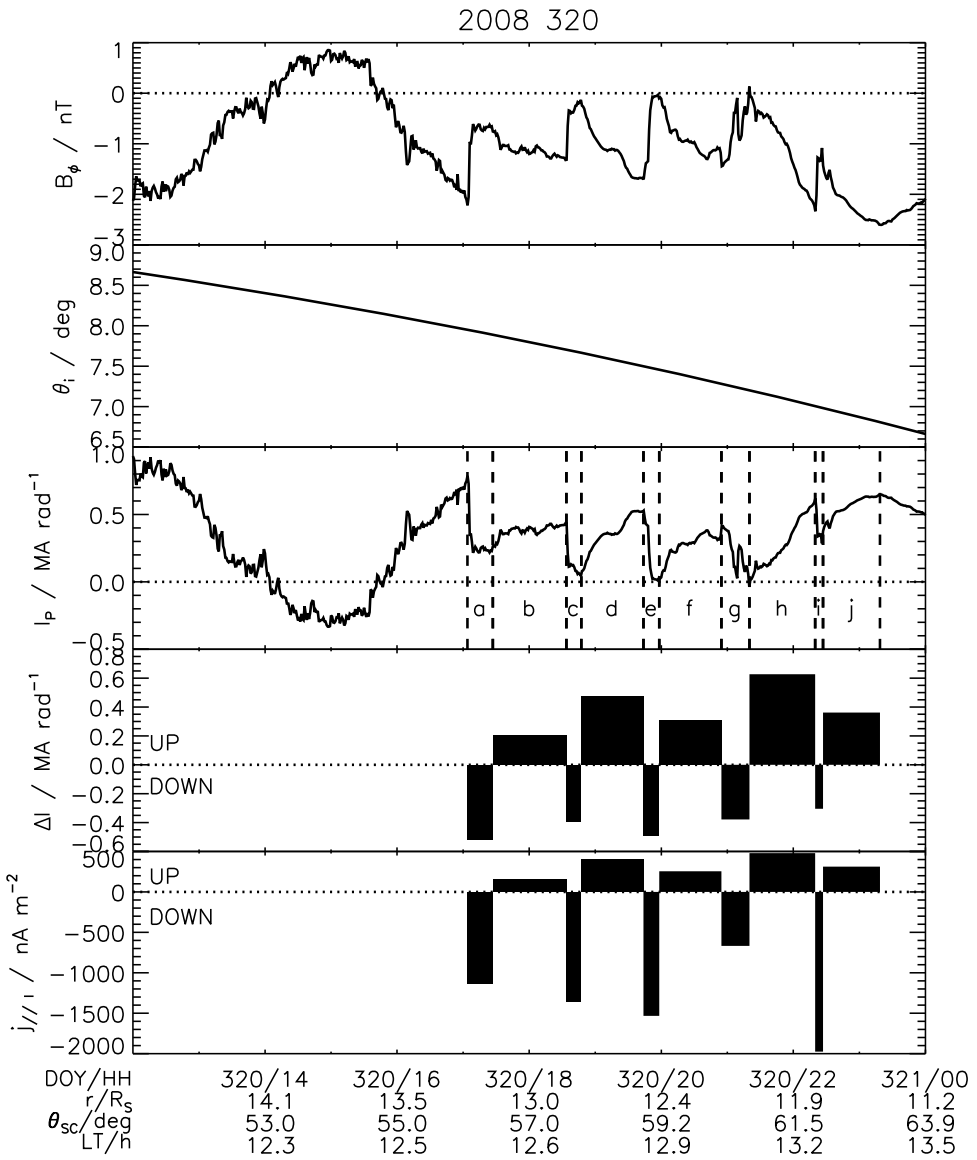

Figure 4. Ionospheric and field-aligned currents. From top to bottom, B_ϕ component of the magnetic field, mapped ionospheric colatitude of Cassini θ_i, height-integrated equatorward ionospheric Pedersen current I_P, field-aligned current ΔI, field-aligned current density just above the ionosphere $j_{\parallel I}$. The vertical dashed lines on Figure 4 (third panel) delimit regions of net increase and decrease in I_P, labeled a–j, which are used to calculate ΔI and $j_{\parallel I}$.

a series of structures encountered by Cassini, rather than a single structure moving back and forth.

2.4. Energetic Electron and Ion Beams

[21] After 12:00 UT on 2008–320 the Magnetospheric Imaging Instrument (MIMI) [*Krimigis et al.*, 2004] Low Energy Magnetospheric Measurements System (LEMMS) and Ion and Neutral Camera (INCA) instruments detected energetic electrons and ions, respectively. These data are plotted in Figure 5 (first and fourth panels), along with field-parallel (0°–20° pitch angle, upward) electron fluxes from ELS (Figure 5, second panel), radio and plasma wave science (RPWS) electric field spectrogram (Figure 5, third panel) and the field-aligned currents derived above (Figure 5, fifth panel). In Figure 5 (first to fourth panels) the vertical dashed lines mark the boundaries of the field-aligned current regions plotted in Figure 5 (fifth panel). The labeled arrow at the top indicates the start time of the VIMS auroral image iii shown in Figure 2a.

[22] The INCA data in Figure 5 (fourth panel) show the fluxes of light ions, which may consist of H^+, H_2^+, H_3^+, He^+ ions but these cannot be distinguished from each other by the instrument. At this time INCA was in neutral mode, meaning it could measure ions with energies above the collimator plate ion rejection cutoff of ~180 keV/q up to the limit of 360 keV/q. The high-energy light ion fluxes show five distinct peaks of 1–2 orders of magnitude greater than the interim values. During this interval the spacecraft was

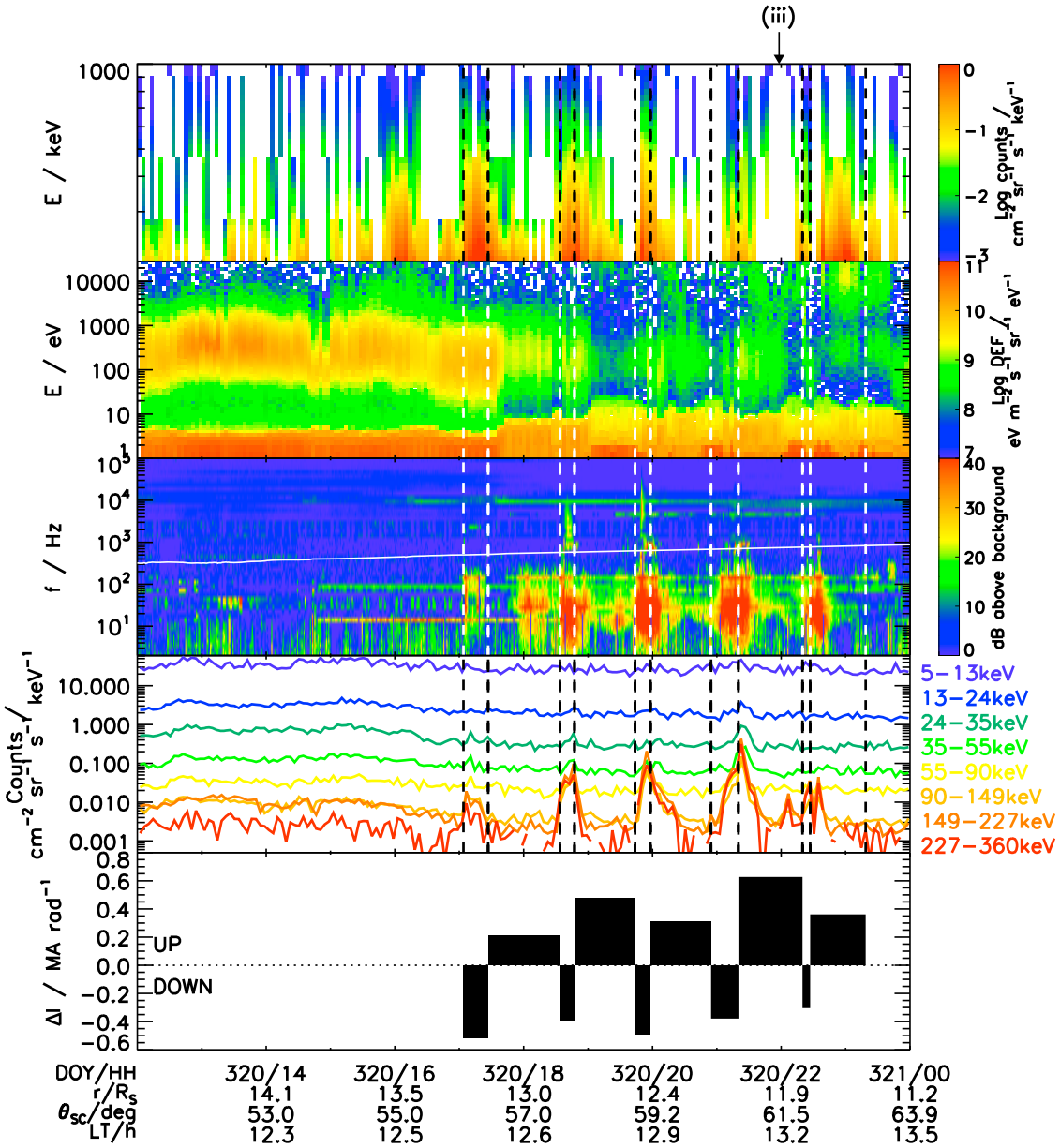

Figure 5. Energetic beams of ions and electrons in regions of field-aligned currents on 2008-320 12:00–24:00 UT. From top to bottom: fluxes of 200 keV to 1 MeV electrons from LEMMS, fluxes of 1 eV to 28 keV field-parallel (upward) electrons from ELS, RPWS electric field spectrogram, ion fluxes measured by INCA, field-aligned current regions determined from MAG data. The vertical dashed lines on first to fourth panels indicate the boundaries of the upward and downward current regions plotted in the fifth panel. The labeled arrow at the top indicates the start time of VIMS auroral image iii shown in Figure 2a.

oriented such that INCA could measure field-aligned ions. The pitch angle distribution of the light ions was strongly focused within ∼30° of the field-parallel (upward from the northern ionosphere) direction.

[23] The ion enhancements were well correlated with the intensifications of the broadband plasma waves shown in Figure 5 (third panel). Most of the wave energy occurred below the electron gyrofrequency (plotted by the white line in Figure 5) indicating that the waves were electromagnetic and propagating in the whistler mode. Poynting vector analysis of the waveforms [*Hospodarsky et al.*, 2001] shows that the waves in these regions were propagating field aligned, i.e., upward from the planet. The narrow beam feature of the ions and the correspondence with the broadband electromagnetic wave enhancements are the same as for the ion conics identified by *Mitchell et al.* [2009a]. At the radial distance sampled in this study, ∼12 R_S, the conic structure had collapsed to form a field-aligned beam. There were also some smaller peaks at lower energies, e.g., 24–35 keV at ∼21:20–21:40 UT. These unusual signatures were

actually caused by energetic heavier ions (e.g., oxygen) entering the sensor above the plate cutoff energy and producing a signal corresponding to lower-energy hydrogen ions. The INCA oxygen channels showed a spike at this time for time-of-flight values corresponding to ion energies in the range 250 keV to over 600 keV. The possible origin of these ions is discussed in section 3.

[24] The LEMMS data (Figure 5, first panel) are shown for an energy range of 200 keV to 1 MeV, i.e., above the upper limit of the ELS measurements. LEMMS measured several intensifications of electrons between ~1600 and 23:30 UT, which were strongest at energies up to ~300 keV. The intensifications lasted from a few min to ~40 min in each case. These were sometimes accompanied by enhancements in the 10 eV to 1 keV electrons measured by ELS and visible in Figure 5 (second panel). Bursts of high-energy electrons were also detected by ELS at ~20:30 UT and throughout 21:00–23:40 UT.

[25] LEMMS was measuring electrons perpendicular to the magnetic field direction such that the high-energy electrons it measured cannot be classed as field-aligned beams. However, previous analyses of similar events have suggested that such electrons have been scattered from a field-aligned beam into larger pitch angles [*Mitchell et al.*, 2009a]. ELS covered pitch angles up to ~110°, i.e., the upward field-parallel direction but not the downward antiparallel direction. The energetic beams detected by ELS were measured in the upward direction only; they are not evident in the field-perpendicular fluxes shown in Figure 3. Past observations have shown both upward and bidirectional electron beams during similar energetic events [*Saur et al.*, 2006; *Mitchell et al.*, 2009a].

[26] The start time of VIMS image iii, 21:58 UT, is marked by the arrow at the top of Figure 5. At this time Cassini's ionospheric footprint is indicated by the white asterisk along the trajectory plotted in Figure 2a. The footprint coincided with an intense poleward auroral arc flanked by narrower dark regions at higher and lower latitudes. The field-aligned current regions plotted in Figure 5 (fifth panel) show that Cassini encountered an upward field-aligned current at this time, enclosed by narrower downward current regions. This confirms the auroral arcs were generated at the foot of upward current regions as expected, while the downward current regions were relatively dark. The relationship of the plasma observations to the field-aligned current regions will be described next.

3. Interpretation of Ion and Electron Beams

[27] The field-aligned current regions plotted in Figure 5 (fifth panel) show repeated adjacent layers of downward and upward currents. The upward ion fluxes and whistler waves exhibit strong enhancements in the downward current regions. The upward acceleration of ionospheric H ions in regions of downward current is consistent with the "pressure cooker" mechanism, whereby the ions are accelerated perpendicular to the magnetic field by wave interactions at low altitude until the mirror force overcomes the parallel electric field trapping them there [e.g., *Carlson et al.*, 1998; *Paschmann et al.*, 2002]. This process leads to a characteristic conic structure of the ions, which collapses to a field-aligned beam at higher altitudes. These structures have been found in the auroral regions of the Earth [*Carlson et al.*, 1998; *Marklund*, 2009] and Saturn [*Mitchell et al.*, 2009a].

[28] The LEMMS data also showed flux enhancements at up to hundreds of keV energies in the downward current regions, which are interpreted to be the scattered upward accelerated electron population. The ELS data showed some enhancements at energies of 10 eV to 1 keV but these were not well correlated with the field-aligned current regions. The ELS data may not show evidence of the upward electrons carrying the downward current because the magnitude of the field-aligned voltage was sufficient to accelerate them to energies above the range detected by ELS (<28 keV). In fact, the high electron energies measured by LEMMS suggest that the field-aligned voltage was of order ~10–100 kV, where wave-particle interactions and scattering may have also contributed to the energization of the electrons.

[29] Turning now to the upward current regions, the energetic electron fluxes measured by LEMMS were reduced in these regions consistent with the downward acceleration of electrons below the spacecraft. There were some enhancements of the warm electron population measured by ELS as mentioned above. The ELS field of view did not include the downward electron population, which was the source of the auroral emission observed. The current carried by the unaccelerated electrons could therefore not be measured in this case.

[30] Cassini observations made on a different pass through Saturn's cusp region have suggested that the current density of the unaccelerated electrons in this region, $j_{\parallel e}$, is a few tens of nA m^{-2} [*Bunce et al.*, 2008a]. This value can be used to estimate the minimum altitude of the acceleration region from $R_{\min}/R_i \approx (j_{\parallel I}/j_{\parallel e})^{1/3}$ (assuming a quasi-dipolar field [e.g., *Cowley et al.*, 2004]). From the magnetic field measurements presented in Figure 4, $j_{\parallel I} \sim 300$ nA m^{-2}. These values yield $R_{\min} \sim 2$ R$_S$, well below Cassini's altitude of ~11 R$_S$. This value is in agreement with previous theoretical studies and observations, which have placed the acceleration region at <1–4 R$_S$ above the planet [*Cowley et al.*, 2004; *Mitchell et al.*, 2009a; *Schippers et al.*, 2011]. Although this estimate is a lower limit, it is reasonable to consider that Cassini was above the acceleration region at this time so would have only encountered the ambient downward electrons, not the accelerated auroral population.

[31] ELS also observed some upward beams of ~keV electrons, e.g., at ~21:40 UT, 22:05 UT, 23:00 UT. *Schippers et al.* [2011] detected upward electrons in a region of upward field-aligned current during an encounter with auroral field lines at Saturn. They related these to very fine downward current structures embedded in the broader upward current regions, which are also evident as brief fluctuations in B_ϕ within the broad current regions defined in the present study (see Figure 4) and may thus explain the energetic electrons observed by ELS.

[32] Our analysis confirms that ion beams (conics at lower altitudes) were generated in regions of downward current identified in the magnetometer data thus supporting the "pressure cooker" acceleration mechanism. The presence of energetic oxygen in the ion beams suggests that the acceleration region extended sufficiently high along the field line above the minimum distances quoted

above to accelerate the ambient oxygen to the energies detected.

4. Discussion

[33] The intense and distinctive auroral structures observed on 2008-320 suggest that this was an interval of highly dynamic magnetospheric activity, which is confirmed by the measurement of energetic ions and electrons on the connected field lines. The location of the auroral intensifications at and poleward of the open-closed field line boundary (the poleward edge of the "main oval"), suggests that they are associated with the creation of open flux and its subsequent antisunward transport. In this interpretation the noon section of the main oval intensifies during an interval of magnetopause reconnection [*Bunce et al.*, 2005a; *Gérard et al.*, 2005]. The main auroral arc then bifurcates as the newly opened flux is transported antisunward (poleward) via the combined effects of solar wind flow and magnetic tension force on the field line [*Milan et al.*, 2000]. The open-closed boundary expands equatorward to accommodate the new open flux. If further bursts of magnetopause reconnection occur, this sequence repeats, leading to a series of auroral arcs poleward of the main oval, which persist until the newly created open flux is assimilated into the tail lobe mapping to the central polar cap. We propose that this is the state that has been captured by Cassini VIMS in Figure 2a some hours into the bursty reconnection interval.

[34] On the basis of this discussion, the observations are now compared to the model results for pulsed dayside reconnection at Saturn obtained by *Bunce et al.* [2005a]. First, to estimate the ionospheric velocity of the auroral arcs, Figure 2a shows that the auroral arcs were ∼1° wide and aligned almost perpendicular to Cassini's antisunward and duskward trajectory. The corresponding upward current regions were encountered by Cassini for approximately 1 h each (Figure 4). During these encounters Cassini's footprint moved approximately 0.2° in the ionosphere. Assuming that the arcs were moving over Cassini in the same direction as its motion, this yields an ionospheric velocity of 1.2° h^{-1} or ∼300 m s^{-1}. This corresponds to the "fast flow" model derived by *Bunce et al.* [2005a], applicable to solar wind compression regions during which the dayside reconnection voltage is ∼400 kV [*Jackman et al.*, 2004].

[35] In the "fast flow" model for subsolar reconnection, a pair of upward and downward directed field-aligned currents are predicted during each burst of reconnection with densities of 300–1300 nA m^{-2} and 70–1000 nA m^{-2}, respectively, depending on the sense of the IMF B_Y component. These ranges encompass the values measured in the present study, remembering that the values shown in Figure 4 would be reduced by factors of ∼5–10 if the widths of the current layers matched the widths of the intense and dark arcs seen in Figure 2a, which were approximately 1°–0.5°. A larger downward current density than upward current density, as measured here, is obtained in the model for IMF $B_Y > 0$ conditions.

[36] *Bunce et al.* [2005a] also derived the field-aligned voltages and resulting auroral emissions in the upward current regions and found that a potential drop of <1–100 kV could be present. In this study the potential drop in the upward current regions cannot be estimated because of the incomplete electron distribution. The fact that upward light ions were not detected in the upward current regions suggests that the field-aligned voltage in these regions was smaller than required to accelerate the ions above the INCA neutral mode cutoff (180 keV/q). In the downward current regions the electron measurements suggest the presence of upward acceleration through tens to hundreds of kV. If the upward field-aligned voltage was of similar magnitude, the associated UV auroral emissions are expected to be ∼10–>100 kR depending on the source electron population [*Bunce et al.*, 2005a]; these are typical to high intensities compared to observations. The lowest latitude arc shown in image iii in Figure 2a was several times more intense than the average IR intensities in this region, while the poleward arcs were of typical "polar" intensities; however the discrete morphology of the poleward arcs is uncommon [*Badman et al.*, 2011b]. These observations are consistent with an energetic driving process occurring at the open-closed field line boundary (lowest latitude arc), which decays over time such that the auroral currents and emissions on higher-latitude (older) open field lines reduce in intensity as the field lines are assimilated into the polar cap.

[37] Finally, the amount of open flux created during the interval can be estimated by measuring the ionospheric area occupied by the bright arcs poleward of the "main oval." Using the method for calculating open flux from auroral images described by [*Badman et al.*, 2005] and the Cassini model of Saturn's magnetic field [*Dougherty et al.*, 2005], the amount of open flux represented by the bright auroral arcs visible within the VIMS FOV shown in Figure 2a is calculated to be ∼7 GWb, which is a significant fraction of the total flux typically threading the polar cap (15–50 GWb [*Badman et al.*, 2005]). Dividing this amount of open flux by the 5 h interval (17:00–22:00 UT) over which the current signatures were observed before VIMS image iii began gives an average dayside reconnection voltage of 390 kV, very similar to the 400 kV quoted above for intervals of strong dayside driving [*Jackman et al.*, 2004].

[38] This value for the reconnection voltage is only an estimate as the duration of the reconnection interval and the surface area occupied by the arcs are not known more precisely, because of Cassini's orbital motion and the incomplete image field of view, respectively. It is in agreement with the apparent equatorward expansion of the auroral oval between images iii and vi; an expansion of ∼1° across the dayside oval as seen between images iii and vi would require the addition of ∼2.4 GWb of open flux. Over the 100 min interval between images iii and vi, this corresponds to an average reconnection rate of 400 kV. Note that this estimate compares measurements of the auroral position from different dayside locations (as VIMS observed different regions in images iii and vi), and assumes that a symmetric expansion of the aurora occurred across all dayside LT over this interval.

[39] This voltage estimate is larger than the 250 kV derived by *Radioti et al.* [2011], who observed a series of poleward auroral arcs over a 2 h interval, indicating stronger driving by the solar wind in the present study. In

fact, 400 kV was the peak reconnection voltage identified during solar wind compression regions by *Jackman et al.* [2004], suggesting that the prevailing conditions during this interval were untypical, e.g., that the IMF magnitude was particularly high. Overall, the similarities of the observations with the *Bunce et al.* [2005a] model lends weight to the interpretation that the field-aligned currents and auroral arcs are signatures of multiple bursts of reconnection at the dayside magnetopause under very strong driving conditions.

[40] Saturn's auroral emissions have also been discussed in relation to vorticity in the magnetosphere and at the magnetopause using both global MHD simulations [*Fukazawa et al.*, 2007] and Cassini observations [*Masters et al.*, 2010]. *Fukazawa et al.* [2007] showed large-scale regions of enhanced electron energy flux and field-aligned currents at high latitude resulting from vortices in the magnetotail or at the magnetopause, but at magnitudes considerably lower than required to produce intense aurora. *Masters et al.* [2010] estimated the auroral signature of a vortex encountered by Cassini at the low-latitude boundary layer but similarly found that it could only generate emission 10–100 times fainter than typical main oval intensities. Recent analysis of high-spatial resolution auroral observations has revealed small spots of UV emission along Saturn's main auroral region, which are suggested to be signatures of successive, traveling Kelvin-Helmholtz vortices [*Grodent et al.*, 2011]. Although these UV spots were observed in the near-noon region, like the IR arcs described in the present study, their morphology was rather different in terms of both size and latitudinal extent. The IR features described in this study are therefore not interpreted as signatures of vortices.

[41] Pulsed and continuous field-aligned ion beams have been commonly observed by Cassini at different LT sectors and L shells [*Mitchell et al.*, 2009a]. While the continuous events may be associated with relatively steady auroral field-aligned currents, the pulsed events may be related to pulsed reconnection at different X line locations as for the event shown here. On the nightside, intermittent reconnection and energization events have been observed in Saturn's magnetotail and are expected to have auroral signatures [*Cowley et al.*, 2005; *Bunce et al.*, 2005b; *Mitchell et al.*, 2009b; *Jackman et al.*, 2010]. During the interval studied here, several characteristics, including the location of the events, suggest they are related to the solar wind interaction and the conversion between closed and open flux, but this will not necessarily be the case for all events. Various dynamic processes, such as flow shears in the low-latitude boundary layer, resulting in auroral field-aligned currents at different LT and latitudes, could produce similar ion and electron beams, but the particle energies and auroral intensities would vary according to the local plasma environment. The global occurrence of these energetic ion and electron beams and their relationship to auroral features requires further detailed study.

5. Conclusions

[42] On 2008-320 Cassini VIMS observed IR auroral arcs in the northern noon sector poleward of the main auroral emission. The arcs are interpreted as the ionospheric signatures of bursts of reconnection occurring at the dayside magnetopause. Each auroral arc was associated with an upward current, i.e., downward flow of electrons into the ionosphere, the magnetic signatures of which were detected by Cassini during this interval. The downward electrons carrying the upward currents were not sampled due to incomplete pitch angle coverage of the plasma instruments but their existence is inferred from the intense auroral arcs at the ionospheric footprint of the field lines. Magnetic and particle observations were made in the downward return current regions, in particular upward bursts of 100–360 keV light ions and energetic (hundreds of keV) electrons, which may have been scattered from upward accelerated beams carrying the downward currents. The light ions were accelerated from low altitudes via the "pressure cooker" mechanism involving acceleration perpendicular to the magnetic field below the field-aligned potential by wave-particle interactions [*Mitchell et al.*, 2009a]. Broadband whistler waves propagating upward were measured by RPWS coincident with the ion bursts. Energetic (600 keV) oxygen ions were also detected, suggesting the presence of ambient oxygen ions within the acceleration region. These simultaneous in situ and remote observations reveal the highly energetic magnetospheric dynamics driving some of Saturn's uncommon auroral features. This is the first in situ identification of transient reconnection events at regions magnetically conjugater to Saturn's magnetopause.

[43] **Acknowledgments:.** This study was facilitated by the Cassini MAG-VIMS collaboration. We acknowledge support of the CAPS ELS science at MSSL-UCL by STFC and of the CAPS ELS operations and software team at MSSL-UCL by STFC (to 2010) and by ESA via UK Space Agency (from 2011). Work at Leicester was supported by STFC grants ST/H002480/1, ST/G002223/1, and PP/E001130/1. The work at the University of Iowa was supported by NASA through contract 1415150 with the Jet Propulsion Laboratory. The authors acknowledge the support of ISSI, as part of this study was discussed by ISSI International Team 178.

[44] Robert Lysak thanks the reviewers for their assistance in evaluating this paper.

References

Arridge, C. S., N. Achilleos, M. K. Dougherty, K. K. Khurana, and C. T. Russell (2006), Modeling the size and shape of Saturn's magnetopause with variable dynamic pressure, *J. Geophys. Res.*, *111*, A11227, doi:10.1029/2005JA011574.

Badman, S. V., E. J. Bunce, J. T. Clarke, S. W. H. Cowley, J.-C. Gérard, D. Grodent, and S. E. Milan (2005), Open flux estimates in Saturn's magnetosphere during the January 2004 Cassini-HST campaign, and implications for reconnection rates, *J. Geophys. Res.*, *110*, A11216, doi:10.1029/2005JA011240.

Badman, S. V., S. W. H. Cowley, J.-C. Gérard, and D. Grodent (2006), A statistical analysis of the location and width of Saturn's southern auroras, *Ann. Geophys.*, *24*(12), 3533–3545.

Badman, S. V., N. Achilleos, K. H. Baines, R. H. Brown, E. J. Bunce, M. K. Dougherty, H. Melin, J. D. Nichols, and T. Stallard (2011a), Location of Saturn's northern infrared aurora determined from Cassini VIMS images, *Geophys. Res. Lett.*, *38*, L03102, doi:10.1029/2010GL046193.

Badman, S. V., C. Tao, A. Grocott, S. Kasahara, H. Melin, R. H. Brown, K. H. Baines, M. Fujimoto, and T. Stallard (2011b), Cassini VIMS observations of latitudinal and hemispheric variations in Saturn's infrared auroral intensity, *Icarus*, *216*, 367–375, doi:10.1016/j.icarus.2011.09.031.

Belenkaya, E. S., I. I. Alexeev, M. S. Blokhina, S. W. H. Cowley, S. V. Badman, V. V. Kalegaev, and M. S. Grigoryan (2007), IMF dependence of the open-closed field line boundary in Saturn's ionosphere, and its relation to the UV auroral oval observed by the Hubble Space Telescope, *Ann. Geophys.*, *25*, 1215–1226, doi:10.5194/angeo-25-1215-2007.

Broadfoot, A. L., et al. (1981), Extreme ulraviolet observations from Voyager-1 encounter with Saturn, *Science*, *212*(4491), 206–211.

Brown, R. H., et al. (2004), The Cassini Visual and Infrared Mapping Spectrometer (VIMS) investigation, *Space Sci. Rev.*, *115*(1–4), 111–168, doi:10.1007/s11214-004-1453-x.

Bunce, E. J., S. W. H. Cowley, and S. E. Milan (2005a), Interplanetary magnetic field control of Saturn's polar cusp aurora, *Ann. Geophys.*, *23*, 1405–1431, doi:10.5194/angeo-23-1405-2005.

Bunce, E. J., S. W. H. Cowley, D. M. Wright, A. J. Coates, M. K. Dougherty, N. Krupp, W. S. Kurth, and A. M. Rymer (2005b), In situ observations of a solar wind compression-induced hot plasma injection in Saturn's tail, *Geophys. Res. Lett.*, *32*, L20S04, doi:10.1029/2005GL022888.

Bunce, E. J., S. W. H. Cowley, C. M. Jackman, J. T. Clarke, F. J. Crary, and M. K. Dougherty (2006), Cassini observations of the Interplanetary Medium Upstream of Saturn and their relation to the Hubble Space Telescope aurora data, *Adv. Space Res.*, *38*, 806–814, doi:10.1016/j.asr.2005.08.005.

Bunce, E. J., S. W. H. Cowley, I. I. Alexeev, C. S. Arridge, M. K. Dougherty, J. D. Nichols, and C. T. Russell (2007), Cassini observations of the variation of Saturn's ring current parameters with system size, *J. Geophys. Res.*, *112*, A10202, doi:10.1029/2007JA012275.

Bunce, E. J., et al. (2008a), Origin of Saturn's aurora: Simultaneous observations by Cassini and the Hubble Space Telescope, *J. Geophys. Res.*, *113*, A09209, doi:10.1029/2008JA013257.

Bunce, E. J., C. S. Arridge, S. W. H. Cowley, and M. K. Dougherty (2008b), Magnetic field structure of Saturn's dayside magnetosphere and its mapping to the ionosphere: Results from ring current modeling, *J. Geophys. Res.*, *113*, A02207, doi:10.1029/2007JA012538.

Carlson, C. W., et al. (1998), FAST observations in the downward auroral current region: Energetic upgoing electron beams, parallel potential drops, and ion heating, *Geophys. Res. Lett.*, *25*, 2017–2020, doi:10.1029/98GL00851.

Clarke, J. T., et al. (2005), Morphological differences between Saturn's ultraviolet aurorae and those of Earth and Jupiter, *Nature*, *433*, 717–719, doi:10.1038/nature03331.

Clarke, J. T., et al. (2009), Response of Jupiter's and Saturn's auroral activity to the solar wind, *J. Geophys. Res.*, *114*, A05210, doi:10.1029/2008JA013694.

Cowley, S. W. H., E. J. Bunce, and J. M. O'Rourke (2004), A simple quantitative model of plasma flows and currents in Saturn's polar ionosphere, *J. Geophys. Res.*, *109*, A05212, doi:10.1029/2003JA010375.

Cowley, S. W. H., S. V. Badman, E. J. Bunce, J. T. Clarke, J.-C. Gérard, D. Grodent, C. M. Jackman, S. E. Milan, and T. K. Yeoman (2005), Reconnection in a rotation-dominated magnetosphere and its relation to Saturn's auroral dynamics, *J. Geophys. Res.*, *110*, A02201, doi:10.1029/2004JA010796.

Crary, F., et al. (2005), Solar wind dynamic pressure and electric field as the main factors controlling Saturn's aurorae, *Nature*, *433*, 720–722, doi:DOI 10.1038/nature03333.

Dougherty, M. K., et al. (2005), Cassini magnetometer observations during Saturn orbit insertion, *Science*, *307*(5713), 1266–1270, doi:10.1126/science.1106098.

Drossart, P., et al. (1989), Detection of H_3^+ on Jupiter, *Nature*, *340*, 539–541.

Fukazawa, K., S. Ogi, T. Ogino, and R. J. Walker (2007), Magnetospheric convection at Saturn as a function of IMF BZ, *Geophys. Res. Lett.*, *34*, L01105, doi:10.1029/2006GL028373.

Gérard, J.-C., D. Grodent, J. Gustin, A. Saglam, J. T. Clarke, and J. T. Trauger (2004), Characteristics of Saturn's FUV aurora observed with the Space Telescope Imaging Spectrograph, *J. Geophys. Res.*, *109*, A09207, doi:10.1029/2004JA010513.

Gérard, J.-C., E. J. Bunce, D. Grodent, S. W. H. Cowley, J. T. Clarke, and S. V. Badman (2005), Signature of Saturn's auroral cusp: Simultaneous Hubble Space Telescope FUV observations and upstream solar wind monitoring, *J. Geophys. Res.*, *110*, A11201, doi:10.1029/2005JA011094.

Grodent, D., J.-C. Gérard, S. W. H. Cowley, E. J. Bunce, and J. T. Clarke (2005), Variable morphology of Saturn's southern ultraviolet aurora, *J. Geophys. Res.*, *110*, A07215, doi:10.1029/2004JA010983.

Grodent, D., J. Gustin, J.-C. Gérard, A. Radioti, B. Bonfond, and W. R. Pryor (2011), Small-scale structures in Saturn's ultraviolet aurora, *J. Geophys. Res.*, *116*, A09225, doi:10.1029/2011JA016818.

Hospodarsky, G. B., T. F. Averkamp, W. S. Kurth, D. A. Gurnett, M. Dougherty, U. Inan, and T. Wood (2001), Wave normal and Poynting vector calculations using the Cassini radio and plasma wave instrument, *J. Geophys. Res.*, *106*, 30,253–30,269, doi:10.1029/2001JA900114.

Huddleston, D. E., C. T. Russell, G. Le, and A. Szabo (1997), Magnetopause structure and the role of reconnection at the outer planets, *J. Geophys. Res.*, *102*, 24,289–24,302, doi:10.1029/97JA02416.

Jackman, C. M., N. Achilleos, E. J. Bunce, S. W. H. Cowley, M. K. Dougherty, G. H. Jones, S. E. Milan, and E. J. Smith (2004), Interplanetary magnetic field at ?9 AU during the declining phase of the solar cycle and its implications for Saturn's magnetospheric dynamics, *J. Geophys. Res.*, *109*, A11203, doi:10.1029/2004JA010614.

Jackman, C. M., C. S. Arridge, J. A. Slavin, S. E. Milan, L. Lamy, M. K. Dougherty, and A. J. Coates (2010), In situ observations of the effect of a solar wind compression on Saturn's magnetotail, *J. Geophys. Res.*, *115*, A10240, doi:10.1029/2010JA015312.

Krimigis, S. M., et al. (2004), Magnetosphere Imaging Instrument (MIMI) on the Cassini Mission to Saturn/Titan, *Space Sci. Rev.*, *114*, 233–329, doi:10.1007/s11214-004-1410-8.

Marklund, G. T. (2009), Electric fields and plasma processes in the auroral downward current region, below, within, and above the acceleration region, *Space Sci. Rev.*, *142*, 1–21, doi:10.1007/s11214-008-9373-9.

Masters, A., et al. (2010), Cassini observations of a Kelvin-Helmholtz vortex in Saturn's outer magnetosphere, *J. Geophys. Res.*, *115*, A07225, doi:10.1029/2010JA015351.

Mauk, B. H., and J. Saur (2007), Equatorial electron beams and auroral structuring at Jupiter, *J. Geophys. Res.*, *112*, A10221, doi:10.1029/2007JA012370.

McAndrews, H. J., C. J. Owen, M. F. Thomsen, B. Lavraud, A. J. Coates, M. K. Dougherty, and D. T. Young (2008), Evidence for reconnection at Saturn's magnetopause, *J. Geophys. Res.*, *113*, A04210, doi:10.1029/2007JA012581.

Melin, H., T. Stallard, S. Miller, J. Gustin, M. Galand, S. V. Badman, W. R. Pryor, J. O'Donoghue, R. H. Brown, and K. H. Baines (2011), Simultaneous Cassini VIMS and UVIS observations of Saturn's southern aurora: Comparing emissions from H, H_2 and H_3^+ at a high spatial resolution, *Geophys. Res. Lett.*, *38*, L15203, doi:10.1029/2011GL048457.

Milan, S. E., M. Lester, S. W. H. Cowley, and M. Brittnacher (2000), Convection and auroral response to a southward turning of the IMF: Polar UVI, CUTLASS, and IMAGE signatures of transient magnetic flux transfer at the magnetopause, *J. Geophys. Res.*, *105*, 15,741–15,755, doi:10.1029/2000JA900022.

Mitchell, D. G., W. S. Kurth, G. B. Hospodarsky, N. Krupp, J. Saur, B. H. Mauk, J. F. Carbary, S. M. Krimigis, M. K. Dougherty, and D. C. Hamilton (2009a), Ion conics and electron beams associated with auroral processes on Saturn, *J. Geophys. Res.*, *114*, A02212, doi:10.1029/2008JA013621.

Mitchell, D. G., et al. (2009b), Recurrent energization of plasma in the midnight-to-dawn quadrant of Saturn's magnetosphere, and its relationship to auroral UV and radio emissions, *Planet. Space. Sci.*, *57*, 1732–1742, doi:10.1016/j.pss.2009.04.002.

Nichols, J. D., B. Cecconi, J. T. Clarke, S. W. H. Cowley, J.-C. Gérard, A. Grocott, D. Grodent, L. Lamy, and P. Zarka (2010), Variation of Saturn's UV aurora with SKR phase, *Geophys. Res. Lett.*, *37*, L15102, doi:10.1029/2010GL044057.

Paschmann, G., S. Haaland, and R. Treumann (2002), In situ measurements in the auroral plasma, in *Auroral Plasma Physics*, *Space Sci. Rev.*, *103*, 93–208, doi:10.1023/A:1023030716698.

Radioti, A., D. Grodent, J.-C. Gérard, S. E. Milan, B. Bonfond, J. Gustin, and W. Pryor (2011), Bifurcations of the main auroral ring at Saturn: Ionospheric signatures of consecutive reconnection events at the magnetopause, *J. Geophys. Res.*, *116*, A11209, doi:10.1029/2011JA016661.

Rijnbeek, R. P., S. W. H. Cowley, D. J. Southwood, and C. T. Russell (1984), A survey of dayside flux transfer events observed by ISEE 1 and 2 magnetometers, *J. Geophys. Res.*, *89*, 786–800, doi:10.1029/JA089iA02p00786.

Saur, J., et al. (2006), Anti-planetward auroral electron beams at Saturn, *Nature*, *439*, 699–702, doi:10.1038/nature04401.

Schippers, P., et al. (2011), Auroral electron distributions within and close to the Saturn kilometric radiation source region, *J. Geophys. Res.*, *116*, A05203, doi:10.1029/2011JA016461.

Slavin, J. A., et al. (2008), Mercury's magnetosphere after MESSENGER's first flyby, *Science*, *321*, 85–89, doi:10.1126/science.1159040.

Stallard, T., et al. (2008), Complex structure within Saturn's infrared aurora, *Nature*, *456*, 214–217, doi:10.1038/nature07440.

Stallard, T. S., S. Miller, L. M. Trafton, T. R. Geballe, and R. D. Joseph (2004), Ion winds in Saturn's southern auroral/polar region, *Icarus*, *167*, 204–211, doi:10.1016/j.icarus.2003.09.006.

Swisdak, M., B. N. Rogers, J. F. Drake, and M. A. Shay (2003), Diamagnetic suppression of component magnetic reconnection at the magnetopause, *J. Geophys. Res.*, *108*(A5), 1218, doi:10.1029/2002JA009726.

Talboys, D. L., E. J. Bunce, S. W. H. Cowley, C. S. Arridge, A. J. Coates, and M. K. Dougherty (2011), Statistical characteristics of field-aligned currents in Saturn's nightside magnetosphere, *J. Geophys. Res.*, *116*, A04213, doi:10.1029/2010JA016102.

Tao, C., S. V. Badman, and M. Fujimoto (2011), UV and IR auroral emission model for the outer planets: Jupiter and Saturn comparison, *Icarus*, *213*, 581–592, doi:10.1016/j.icarus.2011.04.001.

Walker, R. J., and C. T. Russell (1985), Flux transfer events at the Jovian magnetopause, *J. Geophys. Res.*, *90*, 7397–7404, doi:10.1029/JA090iA08p07397.

Young, D. T., et al. (2004), Cassini Plasma Spectrometer investigation, *Space Sci. Rev.*, *114*, 1–112, doi:10.1007/s11214-004-1406-4.

N. Achilleos, Department of Physics and Astronomy, University College London, Gower Street, London WC1E 6BT, UK.

C. S. Arridge and A. J. Coates, Mullard Space Science Laboratory, University College London, Space and Climate Physics, Dorking RH5 6NT, UK.

S. V. Badman, M. Fujimoto, S. Kasahara, T. Kimura, and C. Tao, JAXA Institute of Space and Astronautical Science, 3-1-1 Yoshinodai, Chuo-ku, Sagamihara, Kanagawa 252–5210, Japan. (s.badman@stp.isas.jaxa.jp)

K. H. Baines, SSEC, University of Wisconsin–Madison, 1225 W. Dayton St., Madison, WI 53706, USA.

R. H. Brown, LPL, University of Arizona, 1629 E. University Blvd., Tucson, AZ 85721-0000, USA.

E. J. Bunce, S. W. H. Cowley, H. Melin, and T. Stallard, Department of Physics and Astronomy, University of Leicester, University Road, Leicester LE1 7RH, UK.

M. K. Dougherty, Blackett Laboratory, Imperial College London, Exhibition Road, London SW7 2BZ, UK.

G. Hospodarsky, Department of Physics and Astronomy, University of Iowa, Van Allen Hall, Iowa City, IA 52242, USA.

D. G. Mitchell, APL, Johns Hopkins University, MP3-E132, 11100 Johns Hopkins Rd., Laurel, MD 20723, USA.